CHEMISTRY OF MATERIALS

pubs.acs.org/cm

Article

Understanding Water Enhancement of CO_2 Adsorption in Zeolite Cs−RHO

Hwangho Lee,[‖] Kun-Lin Wu,[‖] Dan Xie, Le Xu, Alexander Okrut, Stacey I. Zones, Ambarish Kulkarni,* and Alexander Katz*

Cite This: *Chem. Mater.* 2024, 36, 11947−11957

Read Online

ACCESS | Metrics & More | Article Recommendations | Supporting Information

ABSTRACT: Structural characterization of humid CO_2 adsorbed in Cs−RHO zeolite was achieved with computationally guided Rietveld refinement, and elucidates the extraordinary enhancement in CO_2 adsorption under wet compared with dry conditions in this zeolite. Our data encompass Rietveld refinement, IR spectroscopy, and molecular simulations, and demonstrate a cooperative effect of water (pulling Cs^+ cations) and CO_2 (pushing Cs^+ cations) in translocating Cs^+ cations away from initial positions in the center of the double eight-membered ring (D8R). This translocation is crucial for unblocking the small-pore RHO framework for CO_2 transport as well as exposing thermodynamically controlled selective sites that can adsorb CO_2 under our humid conditions. Our data emphasize the essentialness of cooperativity in that neither water nor CO_2 achieve this unblocking on their own at 5% relative humidity and 30 °C. These results also demonstrate the importance of multidentate interactions between CO_2 and cations through the D8R, as well as framework oxygen atoms of the D8R, as a key motif in water-resilient CO_2 bonding sites in zeolites, along with additional, weaker interactions with other cations in the alpha cage.

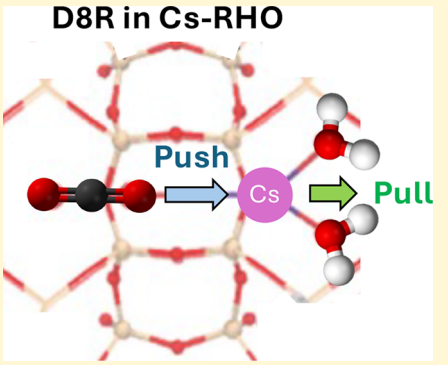

INTRODUCTION

Despite high volumetric dry CO_2 adsorption capacities of zeolites and their desirable weak interactions with CO_2 for energetically facile adsorption/desorption,[1−16] the inevitable presence of water in postcombustion gas streams results in strong competitive adsorption, which decreases CO_2 adsorption capacities.[17−20] Achieving an understanding of the structural features in zeolites that endow thermodynamic water tolerance to CO_2 adsorption sites (i.e., leading to sites that can adsorb humid CO_2 under thermodynamic control) enables an important complementary approach for dealing with water compared to conventional diffusion-based (i.e., kinetic) approaches.[21−23] This understanding is essential for the rational design of zeolites for practical CO_2 capture from postcombustion gas mixtures.[18,23,24]

Sites that can selectively bond CO_2 over water must overcome the generally ∼7 kcal/mol higher affinity of water to zeolites, based on electrostatic interactions and dipole moments that favor water versus CO_2.[20] It has been previously posited that such sites must rely on the higher quadrupolar moment of CO_2 compared with water.[25] In elegant previous work, Lobo et al.[26,27] demonstrated two features of CO_2 bonding sites in small pore zeolites that could interact with the quadrupolar moment of CO_2 by generating electric field gradients: (i) 8-membered ring (8MR) oxygen lone pairs donating electron density to the C atom of CO_2 and (ii) alkali cations acting as a Lewis acid and withdrawing electron density from the O lone pairs of CO_2. This led us to posit that double 8-membered rings (D8R) in zeolites could lead to preferential sites for CO_2 over water. Our recent results with MER, RHO, and PAU zeolites at different Si/Al ratios support the generality of this hypothesis,[28] while emphasizing that adsorption is controlled by the coupled interplay of CO_2, water, the zeolite framework, and the identity of exchange cations.[28−30] Yet when comparing dry versus humid CO_2 adsorption in Cs−RHO, our results go further. They not only indicate a selective bonding site for CO_2 under humid conditions, but they also suggest a high degree of cooperativity between water and CO_2, in increasing adsorption of the latter 3.2-fold compared to dry conditions at 30 °C (see Figures S1 and S2, and Table S1, Supporting Information). Such cooperativity was not observed across other alkali-exchanged cations in the RHO series.[29] Until now, the structural details of this cooperativity have been unknown. Here, relying on a combination of molecular simulation, spectroscopy, and a computationally guided Rietveld refinement of the active site for humid CO_2 adsorption in Cs−RHO, we demonstrate the molecular basis of water−CO_2 cooperativity during humid CO_2 adsorption involving the D8R site. Our results character-

Received: September 5, 2024
Revised: November 5, 2024
Accepted: November 5, 2024
Published: December 13, 2024

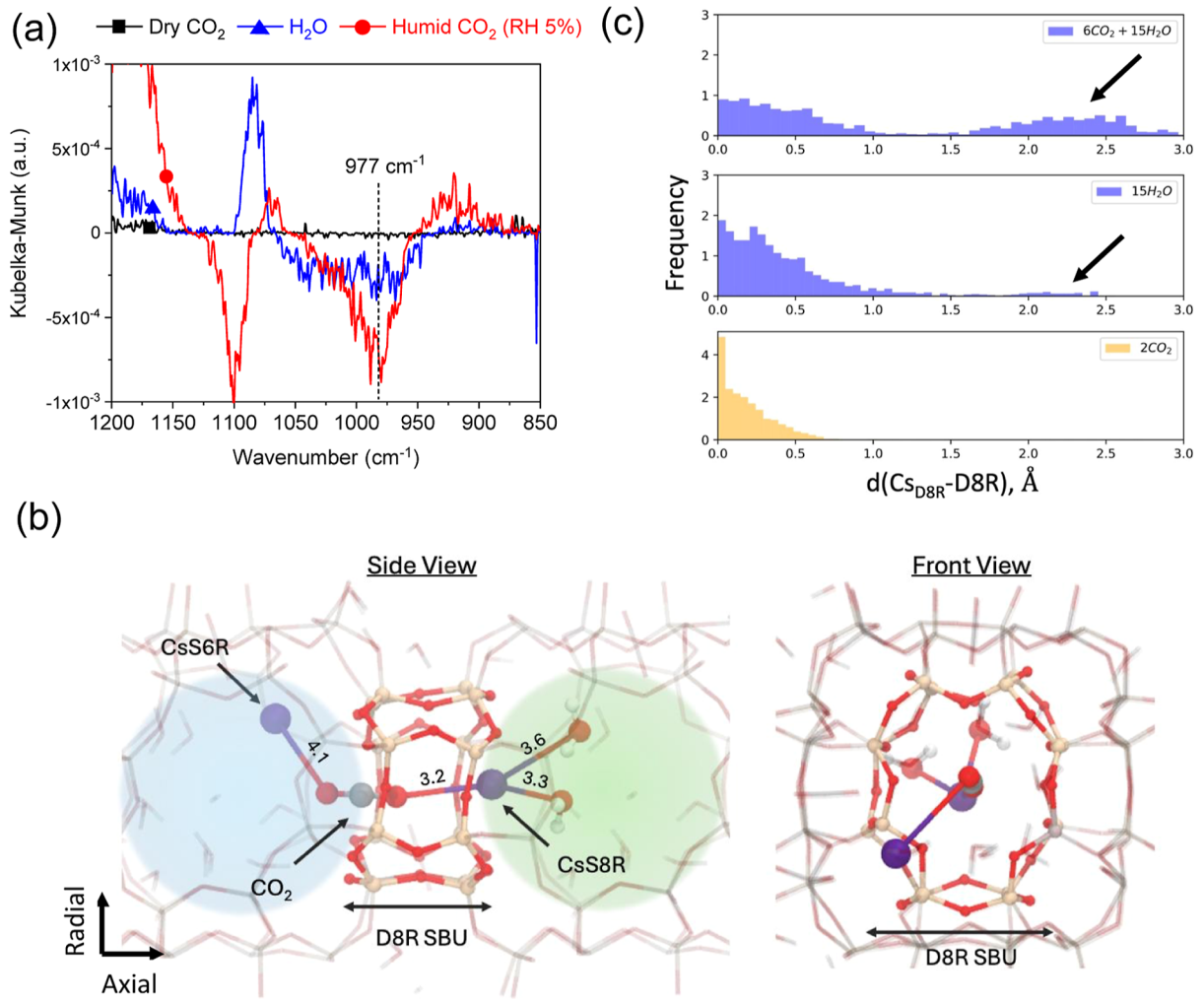

Figure 1. (a) DRIFTS spectra in T−O−T vibration region of Cs−RHO under dry CO_2, humid air (5% RH) and humid CO_2 (5% RH) at 30 °C. (b) Molecular structure of Cs−RHO under humid CO_2 conditions (5% RH, 30 °C) obtained by computationally guided Rietveld refinement. (c) The histogram of Cs_{D8R} displacement from D8R center in the axial direction. Blue histograms represent Cs−RHO with $Im\bar{3}m$ space group (wet) and yellow histogram represents Cs−RHO with $I\bar{4}3m$ space group (dry). The numbers of CO_2 and water correspond to experiment.

ize the structural details of a selective bonding site for humid CO_2 adsorption, which informs the design of water resilient D8R sites observed more generally, in other zeolites (vide supra). These details have until now been unavailable.[28]

Some key questions that this manuscript addresses are (i) how on the molecular length scale do CO_2 and water interact with Cs−RHO so as to account for water enhancing CO_2 adsorption in this material? (ii) What is the structural underpinning of a water-tolerant CO_2 bonding site that endows D8R structures to selectively bond humid CO_2 [i.e., where water (at 5% RH) does not thermodynamically compete with CO_2 under humid conditions]?

Our manuscript builds on prior in situ powder X-ray diffraction (PXRD) data, which demonstrate a phase change in Cs−RHO zeolite upon water and subsequent CO_2 adsorption, at the same relative humidity (RH) of 5% and 1 bar pressure.[29] This phase transition involves a change from the distorted symmetry of the $I\bar{4}3m$ space group in dehydrated Cs−RHO[14,31] to a more symmetric $Im\bar{3}m$ structure after humid CO_2 adsorption, and is similar to ones previously reported by Wright et al.[32] for CO_2 adsorption in Cs−RHO (Si/Al = 3.9) at higher pressures of 4 bar CO_2 under dry conditions. We posited that under our humid CO_2 conditions at 5% RH, water facilitates the translocation of Cs^+ cations away from an initial center of D8R position, toward a distinct single eight-membered ring (S8R) site, at the entrance of the D8R, which opens up the aperture.[33,34] Our results combine structural analysis and direct evidence of interactions between Cs^+ cations and CO_2 via in situ diffuse reflectance infrared Fourier transform spectroscopy (DRIFTS) to demonstrate in detail, on the molecular level, how CO_2 and water, which usually compete for the same adsorption site and hinder the ability of each other to adsorb in zeolites,[17,18] now take on a different role in which they cooperate within the D8R of the Cs−RHO framework to create a water-tolerant CO_2 adsorption site, which functions better wet than dry.

EXPERIMENTAL SECTION

Zeolite Synthesis. Experimental details of synthesis of NaCs−RHO zeolite are available in Supporting Information. Typically, 18-crown-6, Cs−OH solution (50 wt %) and NaOH were dissolved in deionized water. Then, sodium aluminate ($Na_2O{\cdot}Al_2O_3{\cdot}3H_2O$) was added to the mixture, and the solution was stirred until it became clear. Subsequently, colloidal silica (Ludox, AS-40) was added, and the final solution was aged at room temperature for 24 h. The final gel composition of the solution was 1.8 Na_2O:0.3 Cs_2O/Al_2O_3:10 SiO_2:0.5 18-Crown-6:100 H_2O. Hydrothermal synthesis was con-

https://doi.org/10.1021/acs.chemmater.4c02496
Chem. Mater. 2024, 36, 11947−11957

ducted at 125 °C for 3 days under rotation. The resulting zeolite was filtered, washed with deionized water and dried at 80 °C. The as-synthesized zeolite was calcined at 500 °C for 5 h under air flow. The calcined NaCs−RHO zeolite was ion-exchanged with Cs^+ to obtain Cs−RHO.

Characterizations. Single component CO_2 physisorption was performed on an ASAP2020 instrument (Micromeritics) with pure CO_2 gas (99.999%, Praxair). All isotherms were measured at 30 °C after vacuum pretreatment at 350 °C for 4 h. Thermogravimetric analysis (TGA) with a TGA Q5000 (TA Instruments) measured the weight change accompanying humid CO_2 adsorption in Cs−RHO zeolite (Figure S1). In situ DRIFTS was performed with a Tensor 27 (Bruker) (Figure S1). The sample was loaded in a diffuse reflectance cell (Praying Mantis), and pretreated at 350 °C under air for dehydration. Then, the sample was cooled down to 30 °C, and a background spectrum was acquired. With the spectrum of dehydrated Cs−RHO as a background, the time-resolved spectra were obtained during gas adsorption. Experimental details about the quantification of water and CO_2 with combined TGA and DRIFTS are available in Supporting Information.

DFT and AIMD Simulations. Vienna Ab-initio Simulation Package (VASP, version 5.4.4) was used for all density functional theory (DFT) and ab initio molecular dynamics (AIMD) simulations. We used the RPBE functional with a 400 eV plane wave cutoff. The AIMD simulations were performed at 303 K using a 1 fs time step within the *NVT* ensemble. Five different Cs−RHO structures with varying Al distributions were used to model the experimental sample. A total simulation time of at least 20 ps was used. A Nosé−Hoover thermostat with SMASS = 0) was used, which corresponds to a period of 40 time steps. All structure manipulations were performed using the Atomic Simulation Environment (version 3.22.1).

Theory-Guided Rietveld Refinement. DFT was integrated with Rietveld refinement to improve the accuracy and efficiency of structural analysis for Cs−RHO. Whole-pattern profile fitting with the Pawley method was used to obtain the lattice parameters of Cs−RHO sample (14.99 Å). Initial atomistic structures for Cs−RHO were built for DFT calculations using these data. Specifically, we used geometry optimizations with energy change and maximum force thresholds of 1×10^{-6} eV/atom and 0.03 eV/Å, respectively across five ensembles of Al distributions. These DFT-derived atomistic structures served as a starting point for further Rietveld refinement (performed with the TOPAS program) of the Cs−RHO structure containing adsorbed CO_2 and water molecules.

RESULTS AND DISCUSSION

In situ DRIFTS data under dry CO_2 and humid CO_2 (i.e., 5% RH) conditions in Figure 1a show changes to IR bands in the range of 1200−850 cm^{-1}, which represent zeolite-framework T−O−T vibrations (T = Si or Al).[35−37] This spectral region includes a characteristic band at 1050−900 cm^{-1}, which has been previously assigned to perturbations of framework vibrations by the cation and is sensitively affected by changes in the Cs^+-framework interaction ($Cs^+-O_{z,D8R}$, $O_{z,D8R}$ = framework oxygens belonging to the D8R).[38] As such, this vibrational band reports on translocation of the cation away from the center of the D8R.[30] Data in Figure 1a demonstrate what is nearly a flat baseline in the IR subtraction spectrum of Figure 1a under these conditions, showing essentially no change in this spectral window upon dry CO_2 adsorption in Cs−RHO. We conclude that the location of the Cs^+ cation remains largely unperturbed from its known position in dehydrated Cs−RHO, in the center of the D8R.[7,29,32] This observation is consistent with the previously reported lack of change of the $I\bar{4}3m$ space-group symmetry by in situ PXRD for Cs−RHO under 1 bar of dry CO_2, as this symmetry is known to represent a distorted D8R that maximizes strong cumulative cation-zeolite framework interactions, with the Cs^+ cation localized in its center.[32]

These experimental observations are supported by electronic structure calculations relying on density functional theory (DFT). Note that as all the available D8R sites (i.e., 6 D8Rs per unit cell) are occupied by Cs^+ cations, the remaining 4 Cs^+ cations occupy the S6R sites in Cs−RHO. Our electronic structure calculations demonstrate that a Cs^+ cation is bound 0.49 eV stronger within the center of the D8R site in $I\bar{4}3m$ symmetry relative to the analogous site in $Im\bar{3}m$ (see Figure S3, Supporting Information).[39,40] Taken together, our experimental and simulation data are consistent with previous reports,[32] and localize Cs^+ cations in the center of the D8R of Cs−RHO after CO_2 adsorption under dry conditions.

When conducting humid CO_2 adsorption at 5% RH (preceded by water saturation at 5% RH), DRIFTS data in Figure 1a demonstrate the appearance of a strong negative band at 977 cm^{-1}, which was not observed under dry CO_2 conditions above. This negative band in the IR subtraction spectrum arises from the loss of molecular interactions involving the T−O−T framework region, as a result of cation translocation.[30] We surmise that the $Cs^+-O_{z,D8R}$ interaction is weakened as a result of the Cs^+ cation translocation away from its initial position at the center of the D8R, where it is strongly bound to the framework. We observed the same result regardless of whether water and humid CO_2 were adsorbed sequentially versus when they were adsorbed simultaneously, showing path independence, a crucial trait of a system under equilibrium control (see Figure S4, Supporting Information). While such a weakened Cs^+−framework interaction is consistent with our previously reported phase transition accompanying humid CO_2 adsorption, from a distorted $I\bar{4}3m$ to a more symmetric $Im\bar{3}m$ via in situ PXRD as explained above,[29] what has remained unclear is the structural basis for CO_2−water cooperativity at the humid CO_2 adsorption site, involving the translocated Cs^+ cation. This question is all the more crucial given the competing role that water and CO_2 conventionally have in humid CO_2 adsorption, in which water decimates CO_2 adsorption capacities in zeolites. The alternative take that our data brings out is that these two competing species can work together towards the common benefit of humid CO_2 adsorption.

Data from computationally guided Rietveld refinement analysis[41−43] provide the answer to this crucial question. This approach analyzes prior in situ PXRD data under humid CO_2 (5% RH) conditions at 303 K.[29] First, we used conventional Rietveld analysis to obtain approximate atomic positions and occupancies of Cs−RHO for all non-hydrogen atoms. Subsequently, these insights led to an ensemble of five Cs−RHO models ($Si_{38}Al_{10}O_{96}Cs_{10}-6CO_2-15H_2O$) with varying aluminum positions (Si/Al = 3.8), which were used to perform a series of ab initio molecular dynamics (AIMD) simulations (at 303 K for a duration of 20 ps using the RPBE-D3(BJ) functional and VASP software).[44−46] These AIMD trajectories were analyzed to estimate the occupancies of the high symmetry sites for the Cs^+ cations (e.g., D8R, S8R, S6R, and S4R) as well as to obtain the time-averaged positions of the CO_2 and water molecules within the zeolite. These occupancy and position data served as inputs for the next iteration of the Rietveld refinement,[42,43] and the resulting model from the second refinement was then used for DFT-based energy minimizations and further downstream geometric analyses. A key advantage of our iterative DFT-based approach

https://doi.org/10.1021/acs.chemmater.4c02496
Chem. Mater. 2024, 36, 11947−11957

is the ability to resolve the positions of highly mobile species, such as water confined within the zeolite pores, which are typically challenging to deconvolute with conventional Rietveld analysis (see Figure S5, Supporting Information).

The results of our computationally guided Rietveld refinement described above are summarized in Table S2. Referring to the structure shown in Figure 1b, in addition to the Si, Al, O_z, O_{H_2O}, C_{CO_2} and O_{CO_2}, we follow two positions of Cs^+ cations (denoted as Cs_{S8R} and Cs_{S6R} in Table S2 and corresponding to Cs^+ in single 8-ring and 6-ring positions, respectively.) Three key observations from these data enable us to develop a physical picture for this complex system. The first important insight is the similarity between the occupancies and fractional positions of C_{CO_2} (coordinates are [0.5, 0.5, 0.8690]) and the Cs_{S8R} cation (coordinates are [0.5, 0.5, 0.8465]). Based on the crystal symmetry, this suggests that both of these atoms overlap and occupy the same S8R site that is located at the two entrances of the D8R (i.e., 12 S8R sites/unit cell). Second, we note that the number of CO_2 in the framework (i.e., 6 molecules per unit cell), the number of Cs_{S8R} cations (6 cations per unit cell), and number of S8R sites (i.e., 12 per unit cell with an occupancy of 0.5) are all identical in our study. Together, our refinement suggests that all D8Rs of Cs−RHO under 1 bar CO_2 and 5% RH consist of one CO_2 molecule and one Cs^+ cation, which are located at S8R sites. As illustrated in Figure 1b, we conclude that the overlapping fractional positions and identical occupancies of C_{CO_2} and Cs_{S8R} are due to the fact that these atoms straddle the D8R, both of which are located at the S8R site.

From the positions of the O_{H2O}, we surmise that both the Cs_{S8R} and Cs_{S6R} cations mediate the hydrogen bonded water-cluster network within the alpha cage (2 alpha-cages per unit cell).[47,48] We observe that water solvates the Cs^+ cations, which weakens the Cs^+−$O_{z,D8R}$ interaction, and "pulls" the cations to the S8R sites from the D8R center where they initially resided in the $I\bar{4}3m$ space group without CO_2 and water present. These water molecules also interact with the hydrogen bonded water network in the alpha cage (green region in Figure 1b). Simultaneously, the interaction with CO_2 from the adjoining alpha cage "pushes" these Cs^+ cations (Cs^+_{D8R}−O_{CO_2} distance: 3.2 Å) from their original center of D8R locations to the S8R site, further weakening the Cs^+−$O_{z,D8R}$ interactions that are characteristic of the $I\bar{4}3m$ space group. Specifically, as the Cs^+ cation (solvated by both water and CO_2) no longer interacts strongly with $O_{z,D8R}$ atoms, the distorted D8R relaxes to a more symmetric structure that is characteristic of the phase change from $I\bar{4}3m$ to $Im\bar{3}m$ space group alluded to above. Furthermore, Cs^+ cations in the S6R also interact with CO_2 located in S8R sites (denoted by the blue region in Figure 1b), but with a weaker interaction compared to the aforementioned $Cs_{D8R}{}^+$−O_{CO_2} interaction. Taken together, the molecular-level structure above demonstrates a cooperative "push−pull" mechanism involving both CO_2 (pushing Cs^+ cations) and water (pulling Cs^+ cations) facilitating the translocation of Cs^+ cations out of the D8R to the S8R. This mechanism highlights the complex yet cooperative interplay between CO_2, water, and Cs^+ cations in both S8R and S6R sites, leading to CO_2 to be "trapped in door" at the S8R window.

In addition to the interaction with two different Cs^+ cations described above, CO_2 also interacts with surrounding $O_{z,S8R}$ of the framework, with C_{CO_2}−$O_{z,S8R}$ distances spanning 3.0−4.4 Å (see Figure S6, Supporting Information). Several of the $O_{z,S8R}$ can be seen to be close and pointing in toward the C_{CO_2} in Figure 1b. Our observed range of C_{CO_2}−$O_{z,S8R}$ distances is similar to the one previously characterized for CO_2 adsorption in CHA by Lobo et al.[26,27] This C_{CO_2}−$O_{z,S8R}$ is important because it represents oxygen lone-pair donation to adsorbed CO_2, in contrast to the oxygen lone-pair withdrawal by virtue of adsorbed CO_2 interacting with the Lewis acidic Cs^+ cation. Lobo et al. have previously pointed out that similar interactions between dry CO_2 and CHA are together responsible for generating a strong electric field gradient that engages with the quadrupolar moment of CO_2.[26] We surmise that such a "trapped-in-the-door" site can be selective for CO_2 over dipolar water given water's smaller quadrupolar moment.[25]

We now show that the creation of these sites requires both water and CO_2 to be present. Specifically, we used AIMD simulations to investigate three adsorption scenarios: (1) 6 CO_2 and 15 H_2O in Cs−RHO (corresponding to humid CO_2 (5% RH) conditions, $Im\bar{3}m$ topology), (2) 15 H_2O in Cs−RHO (corresponding to humid (5% RH) water-only conditions, $Im\bar{3}m$ topology), and (3) 2 CO_2 (corresponding to dry CO_2-only conditions, $I\bar{4}3m$ topology). This comparison systematically investigates CO_2−water cooperativity in facilitating humid CO_2 adsorption in Cs−RHO. The trajectories from these simulations were characterized by the vector distance of the Cs^+ cation relative to the center of the D8R. The distance vectors are projected as two components, i.e., axial direction (perpendicular to the D8R plane) and radial direction that is orthogonal to the axial component. Here, we focus our discussion on the axial direction as a parameter that differentiates the three scenarios above.[13]

The paragraph below summarizes data from Figure 1c. These data show that a significant fraction of the Cs^+ cations translocate approximately 2.0−3.0 Å out of the D8R center to S8R sites when both water (15 molecules) and CO_2 (6 molecules) are present. In the absence of CO_2, when only 15 molecules of water are present (i.e., no CO_2 coadsorption; middle panel), we observe that the Cs^+ cations largely occupy the center of the D8R—a negligible occupancy of S8R sites is observed. However, a wider distribution of the axial displacements is observed for this water-only case (i.e., 15 H_2O) when compared to the dry case of 2 CO_2 molecules adsorbed within the $I\bar{4}3m$ topology (Figure 1c, bottom panel). The Cs_{D8R} cation is much more localized at the D8R center in the latter case. These results provide further evidence that the hydrogen bonding network from water partially pulls the Cs^+ out of the D8R center, a phenomenon that is synergistic with CO_2 coadsorption because it creates the necessary unsaturation within the Cs^+ coordination sphere that ultimately allows for humid CO_2 bonding, something impossible under dry conditions, when Cs^+ (in the middle of the D8R) is coordinated tightly by the zeolite framework. For completeness, an analogous analysis of 6 CO_2 molecules adsorbed in the $Im\bar{3}m$ and $I\bar{4}3m$ topology is shown in Figure S7, and the higher amount of dry CO_2 does not displace Cs^+ from its preferential D8R positions. We cannot rule out that the small contribution of D8R occupancy observed under humid CO_2 conditions in Figure 1c is due to the limited time scale (20 ps) that is accessible with AIMD. Although the accuracy of our simulations could be improved by using smaller timesteps or by exploring longer simulation times, these studies will require

https://doi.org/10.1021/acs.chemmater.4c02496
Chem. Mater. 2024, 36, 11947−11957

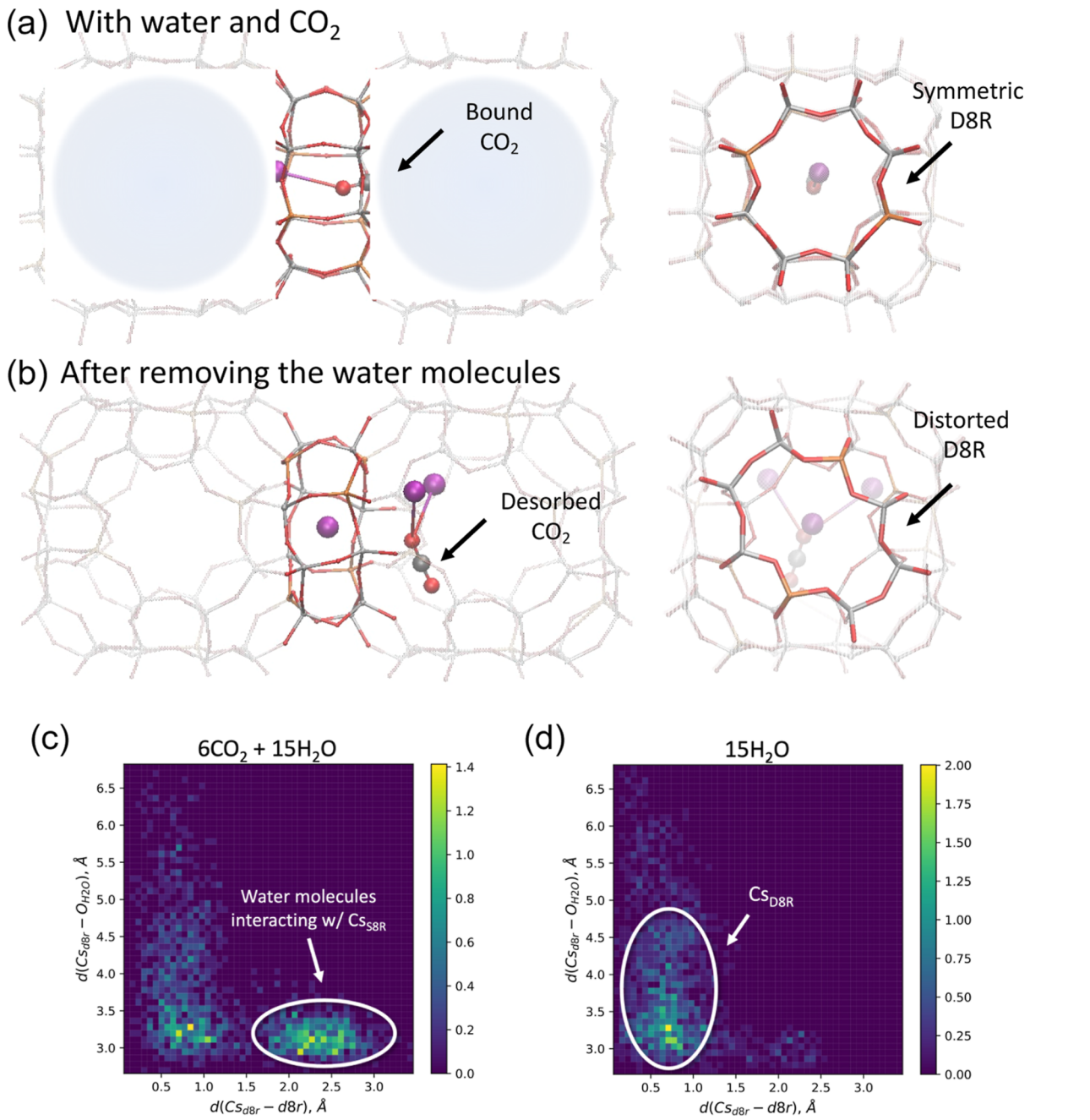

Figure 2. AIMD simulation results of (a) Cs−RHO under humid CO_2 (RH 5%, 30 °C) and (b) Cs−RHO after removing water from the case in (a). (c) and (d) 2D histogram of the Cs_{d8r}−O_{H2O} and Cs_{d8r}−D8R center distances obtained from the simulations in (a) and (b), respectively.

the development of appropriate machine learning potentials[49−51] and are thus beyond the scope of the current study.

From in situ DRIFTS experiments, when water (5% RH) alone adsorbs in Cs−RHO corresponding to case (2) above, without CO_2, we observe only a weak broad band in the IR range of 1000−950 cm^{-1} (Figure 1a, blue trace). This result is qualitatively different from the one observed under humid (5% RH) CO_2 conditions above (Figure 1a, red). Additionally, while only pure single phases are observed under dehydrated conditions in dry air (i.e., $I\bar{4}3m$) and humid CO_2 (i.e., $Im\bar{3}m$) in our previous in situ PXRD data,[29] a complex mixture of phases consisting of both $I\bar{4}3m$ and $Im\bar{3}m$ symmetries was observed for the water-only case. Thus, we surmise that both DRIFTS and our refinement results support the AIMD simulations above, which show that the adsorption of water alone does not cause a complete migration of Cs^+ cations out of the center of D8R to a S8R position—and that such an outcome also cannot be achieved with CO_2 alone. In summary, our combined AIMD simulations and DRIFTS data unequivocally demonstrate that the critical translocation of Cs^+ cations from the center of D8R sites to S8R sites in Cs−RHO at 1 bar requires the cooperative action of both CO_2 and water (5% RH).

We performed two sets of calculations to further illustrate the cooperativity between water and CO_2 on Cs^+ cation translocation, in which the strong interactions between Cs_{D8R}−$O_{z,D8R}$ (under dry CO_2, 1 bar) are replaced by Cs_{S8R}−CO_2 and Cs_{S8R}−water interactions. As a first step, we begin with the

https://doi.org/10.1021/acs.chemmater.4c02496
Chem. Mater. 2024, 36, 11947−11957

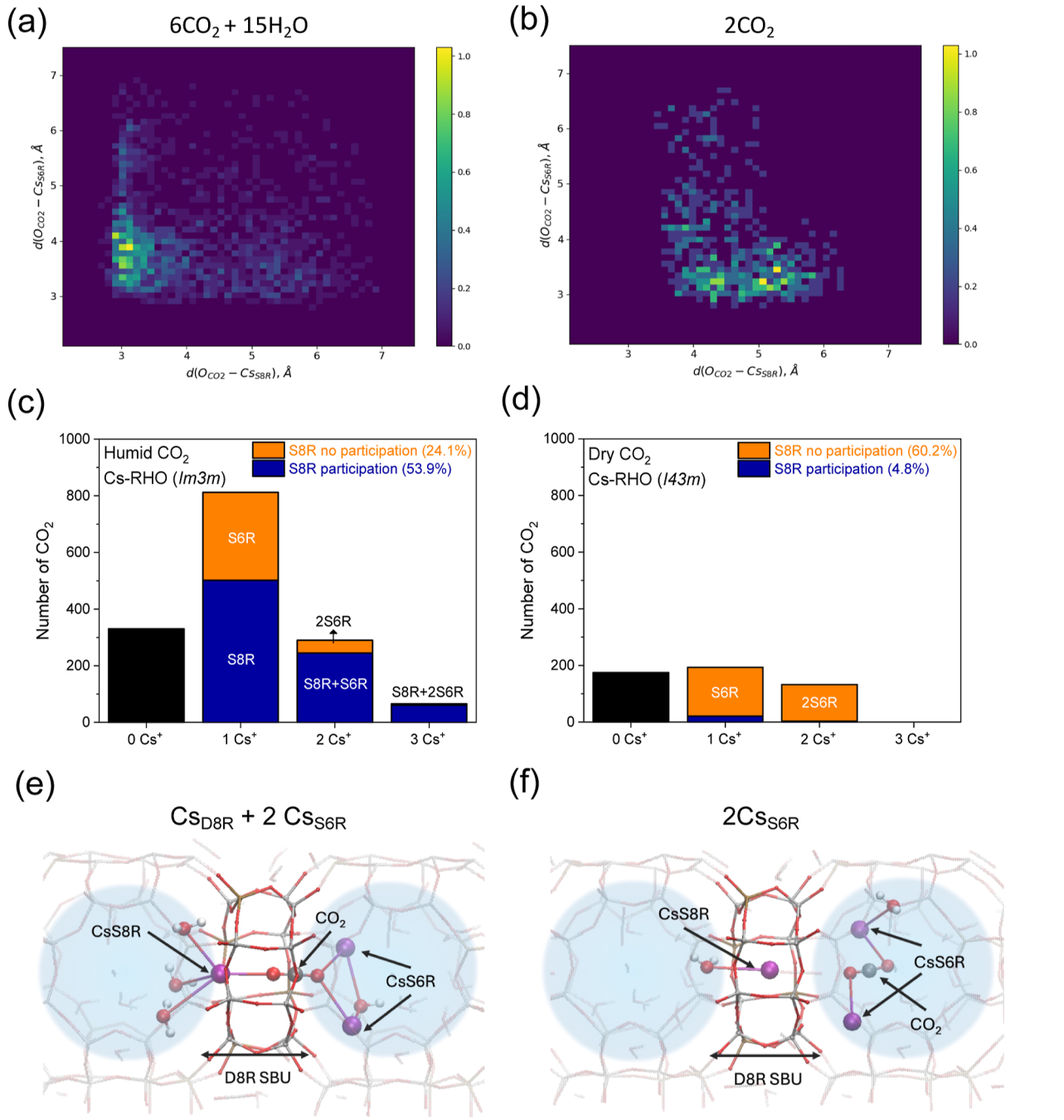

Figure 3. (a,b) 2D histogram of the $Cs_{S8r}-O_{CO_2}$ and $Cs_{S6r}-O_{CO_2}$ distances obtained from the AIMD simulations of Cs−RHO under humid CO_2 (5% RH, 30 °C) and dry CO_2 conditions. (c,d) Bar graphs relating the number of CO_2 to the number of Cs^+ cations interacting with CO_2, under humid CO_2 (5% RH, 30 °C) and dry CO_2 conditions. Parentheses in the legend refer to fractional distribution (e,f) Molecular picture of multidentate Cs^+-CO_2 interaction under humid CO_2 (5% RH, 30 °C) and dry CO_2 conditions, respectively.

refined Cs−RHO structure ($Im\bar{3}m$ space group) and perform a full relaxation using ISIF = 3 in VASP with and without the water molecules present for comparison (Figure 2). For the case that includes the hydrogen-bonded water network, the Cs^+ cations remain in the S8R site, and the D8R remains undistorted as expected for the $Im\bar{3}m$ space group (Figure 2a). However, when the hydrogen bonded water network is removed as shown in Figure 2b, we observe a transition from an initially symmetric D8R site for Cs^+ cations, which is characteristic of the $Im\bar{3}m$ topology, to one that is distorted as in the $I\bar{4}3m$ space group. Concomitantly, in Figure 2b, the Cs^+ cations are "pulled-back" to the center of the D8R site. This results in desorption of the CO_2 molecule, and demonstrates that the hydrogen bonded network (which is mediated by both Cs_{S8R} and Cs_{S6R} cations) along with the presence of CO_2 are essential for Cs^+ translocation from the D8R site to the S8R site. In summary, this rearrangement weakens the interactions of the $O_{z,D8R}$ with the Cs^+ cation, causing relaxation of the D8R to the undistorted state, and ultimately leading to the experimentally observed phase change from $I\bar{4}3m$ (dry conditions) to the $Im\bar{3}m$ space group, when both water (5% RH) and CO_2 are present.

https://doi.org/10.1021/acs.chemmater.4c02496
Chem. Mater. 2024, 36, 11947−11957

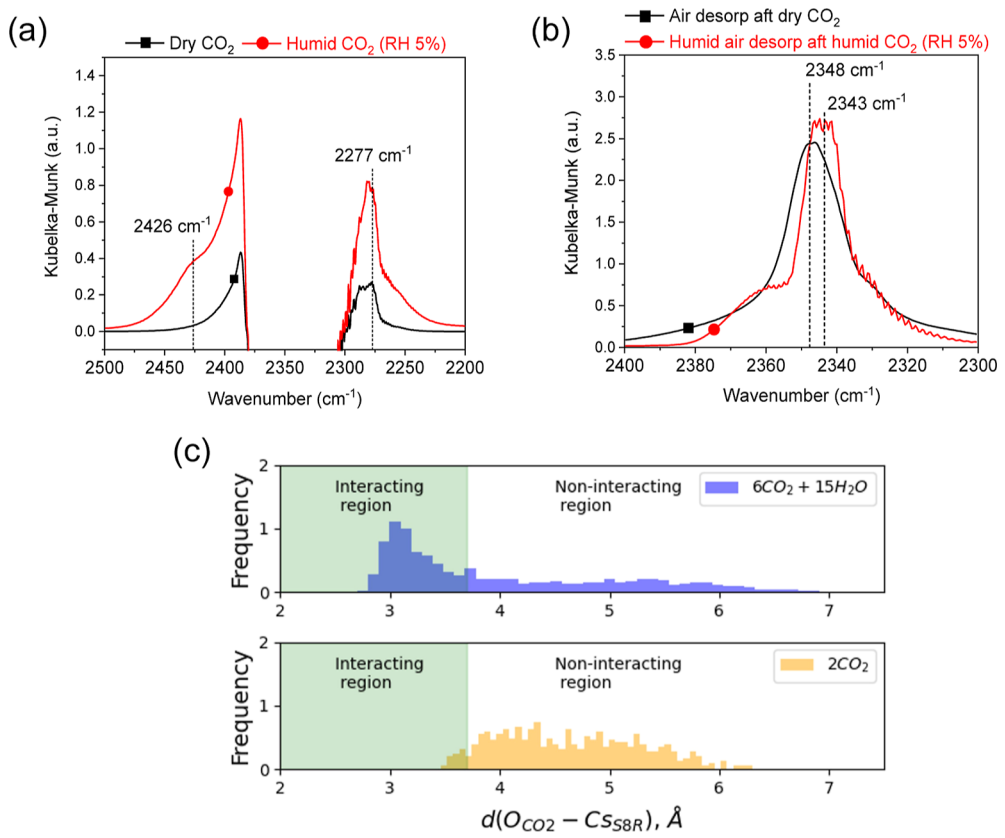

Figure 4. DRIFT spectra of CO_2 adsorbed in Cs−RHO (a) under humid (5% RH) and dry CO_2 conditions at 30 °C followed by (b) respective desorption under humid air (5% RH) and dry air. (c) Histogram of the distribution of Cs_{S8r}−O_{CO_2} distances obtained from the AIMD simulations of the Cs−RHO under (upper panel, blue) humid CO_2 (5% RH, 30 °C) and (lower panel, yellow) dry CO_2 conditions. The amount of CO_2 and water in the simulations correspond to experimental results.

Using the aforementioned AIMD trajectories, we have also investigated the effect of CO_2 adsorption on the hydrogen bond network within the alpha cage. First, as shown in Figure 2c,d, we note that water molecules are mostly located >3 Å away from the $D8R_{center}$, indicating that the D8R is not a preferred site for water adsorption in the presence of humid CO_2 (5% RH). Second, on addition of CO_2, we see the formation of a new peak during water and CO_2 coadsorption in Figure 2c, which is absent for the case of a humid (5% RH) atmosphere without CO_2 in Figure 2d. This region corresponds to water molecules that bond to Cs_{S8R} cations, which have been displaced from their D8R sites. This translocation, as discussed above, is facilitated by CO_2 localization at the entrance to the D8R and explains the experimentally observed increase in CO_2 adsorption in the presence of water. This phenomenon of the D8R providing a selective site for humid CO_2 adsorption is also observed in our recent report involving K-RHO as well as K-MER and K-PAU, where CO_2 adsorption desorbs water from the D8R.[28,30]

During our investigation into CO_2 trapped in the door of Cs−RHO under wet conditions, a fundamental question surfaces—does the structural configuration ensuring CO_2 stability within the D8R sites endure consistently? To address this question comprehensively, we conducted an in-depth geometric analysis employing AIMD trajectories. Notably, our study encompasses an exploration of the interactions with Cs^+ cations adjacent to S6R sites, and uncovers the importance of dual and, in general, multiple cation interactions.[52−57] From this perspective, CO_2 acts as a bridge between Cs_{S8R} and Cs_{S6R} cations within the alpha cage, introducing a dynamic element to the trapping mechanism. Within the Cs−RHO structure, 10 Cs^+ cations are strategically distributed, with 6 positioned at Cs_{S8R} and the remaining 4 at Cs_{S6R} sites. This distribution pattern, coupled with the presence of 8 S6R windows per alpha cage, suggests a structural limitation, indicating that not all CO_2 molecules can simultaneously bind to both Cs_{S6R} and Cs_{S8R}. The simulation results thus bring forth a more nuanced understanding: the stability of CO_2 "trapped in the door" hinges on its proximity to both Cs_{S8R} and Cs_{S6R}, while Cs^+ retains its fixed position at S8R locations.

To unravel the frequency and nature of CO_2 interactions with Cs_{S8R} and Cs_{S6R} within wet Cs−RHO, we meticulously constructed 2D histograms of the AIMD trajectories, by examining the distances between Cs_{S8R}−O_{CO_2} and Cs_{S6R}−O_{CO_2} for water and CO_2 coadsorption ($Im\bar{3}m$ topology, Figure 3a) and dry CO_2 ($I\bar{4}3m$ symmetry, Figure 3b). In the histograms, we use a distance of 3.7 Å as the threshold for defining a Cs^+−O_{CO_2} interaction, which encompasses the range of experimentally measured Cs^+−O_{CO_2} distances in previous zeolite studies and experimental X-ray diffraction measurements.[58] First, we observe that the interaction of humid CO_2 is stronger with Cs_{S8R}, as evidenced by shorter Cs_{S8R}−O_{CO_2} average distances (i.e., 3.2 Å) than those with Cs_{S6R} (i.e., 3.8 Å). These results paint a dynamic picture, revealing that in nearly 72% of instances (Figure 3c), humid CO_2 engages with either Cs_{S6R}, Cs_{S8R}, or both, thereby corroborating the persistence of the "trapped in the door" phenomenon. Figure 3e shows an

https://doi.org/10.1021/acs.chemmater.4c02496
Chem. Mater. 2024, 36, 11947−11957

extreme case of tridentate interactions involving humid CO_2 interacting with three different Cs^+ cations (see Supporting Information, Movie S1). Additionally, as shown in Movie S2, under wet conditions, we sometimes observe a CO_2 molecule desorbing and transitioning into the alpha cage. When this occurs, we observe the Cs_{S8R}, now devoid of CO_2, simultaneously reverting from its S8R site to the D8R site, prompting the closure of the open door. This dynamic process highlights the weak nature of the interactions (which are desirable for CO_2 storage and release) and the intricate interplay between CO_2 and Cs^+ cations at different sites.

Conversely, our comparative analysis for dry Cs−RHO (2 CO_2 per unit cell, $I\bar{4}3m$ symmetry) in Figure 3d shows that one-third of CO_2 molecules interact with neither Cs_{D8R} nor Cs_{S6R}, while one-fourth of CO_2 interacts with two Cs_{S6R} (as shown in Figure 3f). The relative fraction of all of these outcomes was significantly lower for humid CO_2 adsorption in Cs−RHO in Figure 3c. The analysis further reveals nearly no instances where dry CO_2 interacts with both Cs_{S6R} and Cs_{S8R}, as well as a decrease in interactions with $Cs_{S8R/D8R}$ solely (54% and 39% of CO_2 molecules in the system for humid and dry CO_2 adsorption, respectively). These results are consistent with our experimental data in Figure 1a, which show the absence of a framework perturbation band for the dry CO_2 case in Cs−RHO (vide supra), and are further reinforced with additional IR data in Figure 4a below. The data correlate the framework perturbation band and motion of the Cs^+ cation out of the D8R, both of which are observed under humid CO_2 conditions.

We turn again to DRIFTS to investigate the interactions of CO_2 with the Cs^+ cation under dry and humid conditions, focusing on IR bands in the region of 2500−2200 cm^{-1}, which are assigned to an asymmetric stretching (ν_3) of physisorbed CO_2 and gas phase CO_2.[59−62] We note in passing a lack of observed chemisorbed (carbonate) bands (these possess multiple vibrational bands in the spectral window of 1600−1300 cm^{-1})[62−65] under both our dry and humid CO_2 conditions (see Figure S8, Supporting Information).

We rely on gas-phase CO_2 (i.e., no zeolite in the DRIFTS cell) as a baseline for acquiring subtraction IR spectra (see details in Figure S9, Supporting Information) shown in Figure 4a. These data demonstrate an increase in intensity at 2277 cm^{-1} during CO_2 adsorption under both humid (5% RH) and dry conditions. We assign this to the asymmetric stretch of physisorbed $^{13}CO_2$ in Cs−RHO, which is present at a natural abundance of around 1%. The observed sharp band at 2385 cm^{-1} is a subtraction artifact resulting from the tail of the high-intensity $^{12}CO_2$ asymmetric stretch. The characteristic band at 2426 cm^{-1} shown for Cs−RHO under humid CO_2 (5% RH) conditions in Figure 4a is assigned to a combination band ($\nu_3 + \nu_{is}$, ν_{is} indicates vibration of $Cs^+\cdots O$ in $Cs^+\cdots O{=}C{=}O$),[59,61] which includes contributions from a Cs^+-CO_2 interaction as well as the asymmetric stretch of $^{12}CO_2$. The observed increase in the intensity of this band upon humid CO_2 adsorption provides direct evidence for CO_2 interacting with Cs^+ cation under humid CO_2 conditions in Cs−RHO. Importantly, we observed no 2426 cm^{-1} band intensity after dry CO_2 adsorption in Figure 4a. We conclude that while some CO_2 adsorption occurs in Cs−RHO under dry conditions (see Figure S2c, Supporting Information), it does not arise due to strong CO_2 interactions (as measured by DRIFTS) with the Cs^+ cation. We emphasize that these strong interactions are only possible under humid CO_2 conditions. Consistent with equilibrium control, the same Cs^+-CO_2 interaction is achieved, regardless of whether water (5% RH) and CO_2 are introduced sequentially or whether they are adsorbed simultaneously (see Figure S10, Supporting Information). Even at a lower CO_2 concentration corresponding to that in flue gas (15% CO_2 in humid air at 5% RH), we still observe the presence of a Cs^+-CO_2 interaction during humid CO_2 adsorption, as shown in Figure S11. These data clearly demonstrate that cooperativity between water and CO_2 is still functional even at these more dilute, practical conditions.

Note that we were unable to analyze the IR band corresponding to $^{12}CO_2$ asymmetric stretching at 2375−2300 cm^{-1} because of a large competing absorbance from gas-phase $^{12}CO_2$ in this spectral window (i.e., the gas-phase CO_2 saturates the IR detector and makes its reliable subtraction impossible). However, we were able to resolve the ν_3 of $^{12}CO_2$ during desorption under carrier (air) gas flow because there is a lack of interference from gas-phase CO_2 under this condition (Figure 4b). The IR difference spectra obtained during this desorption consist of bands at 2348 and 2343 cm^{-1} under dry and wet conditions, respectively, which we assign to physisorbed $^{12}CO_2$. The two slightly different frequencies imply different environments for adsorbed CO_2 depending on the presence or absence of coadsorbed water. The nearly identical IR frequency of 2348 cm^{-1} under dry CO_2 conditions compared with free gas-phase CO_2 (i.e., 2349 cm^{-1}) demonstrates little interaction of CO_2 with Cs−RHO zeolite in the absence of water. In contrast, under humid conditions, the lower frequency observed for the $^{12}CO_2$ asymmetric stretch implies that the C−O bond is weakened under these conditions, which coincides with the previously reported IR frequency of CO_2 interacting with Cs^+ cations in zeolite Cs-ZSM-5.[61] The observed C−O bond weakening may be of interest for catalytic applications. This result further reinforces a strong interaction between Cs^+ cations and physisorbed CO_2 in Cs−RHO uniquely when water is present, under humid conditions, with these interactions being absent under dry conditions.

To further support cooperativity of water and CO_2 being the key factor that causes Cs^+ migration away from its D8R location in Cs−RHO, we performed a geometric analysis to examine the interaction of CO_2 with the Cs^+ cations near D8R sites using AIMD. The distance histograms in Figure 4c for Cs−RHO correspond to our two experiments: (1) humid CO_2 conditions corresponding to 6 CO_2 and 15 H_2O adsorbed in Cs−RHO with $Im\bar{3}m$ topology, and (2) dry CO_2 conditions corresponding to 2 adsorbed CO_2 molecules in Cs−RHO with $I\bar{4}3m$ structure. Using established criteria for a $Cs^+-O_{CO_2}$ bond (i.e., 2.46−3.60 Å), we identified the Cs^+ cation and CO_2 interacting region in the histogram with $Cs^+-O_{CO_2}$ to be less than 3.70 Å in Figure 4c. We observed an interaction between Cs^+ cations at S8R positions and CO_2 only under humid conditions. In stark contrast, under dry conditions, we see nearly no evidence of CO_2 interactions with Cs^+ near D8R positions, and instead observe CO_2 diffusing more freely in the alpha cage of Cs−RHO. The lack of water-cluster hydrogen bonding network prevents Cs^+ from being displaced out of the D8R center, and there are no opportunities for CO_2 to be held at the S8R site forming the "trapped in the door" bonding motif, as shown in Figure 1b. Since there are no spaces for CO_2 to be adsorbed, this rationalizes the observed lower uptake of CO_2 in Cs−RHO under dry versus wet conditions.

https://doi.org/10.1021/acs.chemmater.4c02496
Chem. Mater. 2024, 36, 11947−11957

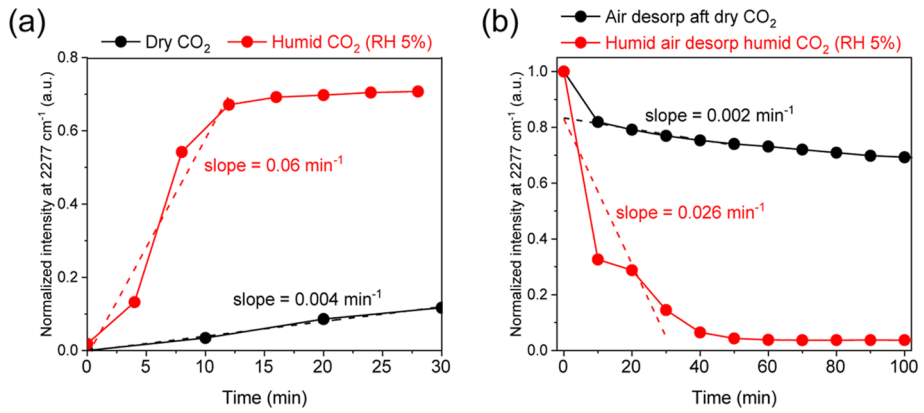

Figure 5. Time-dependent intensity profile of adsorbed CO_2 (monitored by the IR band of $^{13}CO_2$ at 2277 cm^{-1}) during (a) adsorption and (b) desorption of CO_2 under both humid (5% RH) and dry conditions at 30 °C.

Taken together, our integrated experimental and molecular simulation-based observations lead us to conclude that cooperativity between water and CO_2 contributes two characteristic features for facilitating CO_2 adsorption under humid conditions in Cs−RHO, enabling: (i) a Cs^+−CO_2 interaction and (ii) Cs^+ migration out of the middle of the D8R, which both enhance the capacity of the zeolite for adsorption of CO_2 when under wet rather than dry conditions. These two characteristics occur in conjunction with each other. The phenomena are intriguing in that water facilitates CO_2 adsorption at the S8R site as well as interaction with the Cs^+ cation, instead of the conventional role of water competing with CO_2 for a bonding site in the zeolite.[17,18]

Building on the demonstrated cooperativity between CO_2 and water in translocating Cs^+ cations from the middle of the D8R to a S8R position, we investigate how this translocation influences the kinetics of CO_2 adsorption in Cs−RHO. During transient desorption of CO_2 in a humid air environment, the intensity of physisorbed $^{13}CO_2$ bands (which are also correlated with a $^{12}CO_2$ band presence—see Figure S12c, Supporting Information) exhibit a linear correlation with the Cs^+−CO_2 band at 2426 cm^{-1} (see Figure S12d, Supporting Information). The uniformity represented by this linear correlation suggests that a majority of the physisorbed CO_2 interacts with Cs^+ cations, which is consistent with the AIMD simulation results under humid CO_2 conditions in Figure 3c. Data in Figure 5 demonstrate the adsorption/desorption kinetics for dry and humid CO_2 that are reflected by dynamic intensity profiles of $^{13}CO_2$ bands at 2277 cm^{-1} (for the raw spectra, see Figure S13, Supporting Information). These data demonstrate a 15-fold increased rate of CO_2 adsorption/desorption under wet compared to dry conditions. Although kinetic rather than thermodynamic in nature (in contrast to the data of Figure 4a), these data show the internal-diffusion effect of opening the D8R via Cs^+ cation translocation to the S8R, as a consequence of our described cooperative action of water and CO_2 above. Based on these data, we posit that the rate limiting step for the diffusion under dry conditions involves translocation of the Cs^+ cation away from its position at the center of the D8R. When the D8R is unblocked by Cs^+ in the presence of water and CO_2, it opens up the D8R as a portal to the alpha cage. We anticipate that these insights into the critical importance of CO_2−water cooperativity for enabling faster transport kinetics may be transferable to other zeolite systems, such as Na−RHO, which has been reported to exhibit extraordinarily slow dry CO_2 transport.[66]

CONCLUSIONS

Our results provide molecular structural characterization of CO_2−water cooperativity during humid CO_2 adsorption in the D8R site of Cs−RHO. This characterization was performed with multiple techniques: (i) in situ DRIFTS, (ii) Rietveld refinement of in situ PXRD data, and (iii) ab initio molecular dynamics (AIMD). More generally, our data structurally elucidates D8R sites as water-tolerant CO_2 bonding sites. Our data also provide insight into the enhanced kinetics of CO_2 adsorption under wet versus dry conditions.

ASSOCIATED CONTENT

Data Availability Statement

Data are available from the corresponding authors upon request.

Supporting Information

The Supporting Information is available free of charge at https://pubs.acs.org/doi/10.1021/acs.chemmater.4c02496.

Experimental details, DRIFT spectra, TGA data (PDF)

Movie S1 and Movie S2 (ZIP)

AUTHOR INFORMATION

Corresponding Authors

Ambarish Kulkarni − *Department of Chemical Engineering, University of California, Davis, California 95616, United States;* orcid.org/0000-0001-9834-8264; Email: arkulkarni@ucdavis.edu

Alexander Katz − *Department of Chemical and Biomolecular Engineering, University of California, Berkeley, California 94720, United States;* orcid.org/0000-0003-3487-7049; Email: askatz@berkeley.edu

Authors

Hwangho Lee − *Department of Chemical and Biomolecular Engineering, University of California, Berkeley, California 94720, United States;* orcid.org/0000-0001-5756-9722

Kun-Lin Wu − *Department of Chemical Engineering, University of California, Davis, California 95616, United States*

Dan Xie − *Chevron Technology Center, Richmond, California 94801, United States;* Present Address: Braskem

Renewable Innovation Center, Lexington, Massachusetts 02421, United States; orcid.org/0000-0003-2467-976X
Le Xu − *Department of Chemical and Biomolecular Engineering, University of California, Berkeley, California 94720, United States*
Alexander Okrut − *Department of Chemical and Biomolecular Engineering, University of California, Berkeley, California 94720, United States*
Stacey I. Zones − *Chevron Technology Center, Richmond, California 94801, United States;* orcid.org/0000-0002-3128-6481

Complete contact information is available at: https://pubs.acs.org/10.1021/acs.chemmater.4c02496

Author Contributions

‖H.L. and K.-L.W. contributed equally to this work.

Notes

The authors declare no competing financial interest.

■ ACKNOWLEDGMENTS

The authors gratefully acknowledge funding from the CeRCaS NSF IUCRC for all synthesis and molecular modeling aspects related to this work, and DOE, Office of Basic Energy Sciences (DE-FG02-05ER15696) for all characterization aspects including TGA and DRIFTS.

■ REFERENCES

(1) Chen, K.; Mousavi, S. H.; Singh, R.; Snurr, R. Q.; Li, G.; Webley, P. A. Gating effect for gas adsorption in microporous materials-mechanisms and applications. *Chem. Soc. Rev.* **2022**, *51* (3), 1139−1166.
(2) Fu, D.; Davis, M. E. Carbon dioxide capture with zeotype materials. *Chem. Soc. Rev.* **2022**, *51* (22), 9340−9370.
(3) McDonald, T. M.; Mason, J. A.; Kong, X.; Bloch, E. D.; Gygi, D.; Dani, A.; Crocella, V.; Giordanino, F.; Odoh, S. O.; Drisdell, W. S.; et al. Cooperative insertion of CO2 in diamine-appended metal-organic frameworks. *Nature* **2015**, *519* (7543), 303−308.
(4) Zhao, J.; Mousavi, S. H.; Xiao, G.; Mokarizadeh, A. H.; Moore, T.; Chen, K.; Gu, Q.; Singh, R.; Zavabeti, A.; Liu, J. Z.; et al. Nitrogen rejection from methane via a "trapdoor" K-ZSM-25 zeolite. *J. Am. Chem. Soc.* **2021**, *143* (37), 15195−15204.
(5) Haszeldine, R. S. Carbon capture and storage: how green can black be? *Science* **2009**, *325* (5948), 1647−1652.
(6) Hudson, M. R.; Queen, W. L.; Mason, J. A.; Fickel, D. W.; Lobo, R. F.; Brown, C. M. Unconventional, highly selective CO2 adsorption in zeolite SSZ-13. *J. Am. Chem. Soc.* **2012**, *134* (4), 1970−1973.
(7) Lozinska, M. M.; Mangano, E.; Mowat, J. P.; Shepherd, A. M.; Howe, R. F.; Thompson, S. P.; Parker, J. E.; Brandani, S.; Wright, P. A. Understanding carbon dioxide adsorption on univalent cation forms of the flexible zeolite Rho at conditions relevant to carbon capture from flue gases. *J. Am. Chem. Soc.* **2012**, *134* (42), 17628−17642.
(8) Shang, J.; Li, G.; Singh, R.; Gu, Q.; Nairn, K. M.; Bastow, T. J.; Medhekar, N.; Doherty, C. M.; Hill, A. J.; Liu, J. Z.; et al. Discriminative separation of gases by a "molecular trapdoor" mechanism in chabazite zeolites. *J. Am. Chem. Soc.* **2012**, *134* (46), 19246−19253.
(9) Choi, H. J.; Min, J. G.; Ahn, S. H.; Shin, J.; Hong, S. B.; Radhakrishnan, S.; Chandran, C. V.; Bell, R. G.; Breynaert, E.; Kirschhock, C. E. A. Framework flexibility-driven CO2 adsorption on a zeolite. *Mater. Horiz.* **2020**, *7* (6), 1528−1532.
(10) Bruce, E. L.; Georgieva, V. M.; Verbraeken, M. C.; Murray, C. A.; Hsieh, M.-F.; Casteel, W. J.; Turrina, A.; Brandani, S.; Wright, P. A. Structural Chemistry, Flexibility, and CO2 Adsorption Performance of Alkali Metal Forms of Merlinoite with a Framework Si/Al Ratio of 4.2. *J. Phys. Chem. C* **2021**, *125* (49), 27403−27419.
(11) Choi, S.; Drese, J. H.; Jones, C. W. Adsorbent materials for carbon dioxide capture from large anthropogenic point sources. *ChemSusChem: Chemistry & Sustainability Energy & Materials* **2009**, *2* (9), 796−854.
(12) Pacala, S.; Al-Kaisi, M.; Barteau, M.; Belmont, E.; Benson, S.; Birdsey, R.; Boysen, D.; Duren, R.; Hopkinson, C.; Jones, C. *Negative Emissions Technologies and Reliable Sequestration: A Research Agenda*; National Academies of Sciences, Engineering, and Medicine, 2018.
(13) Coudert, F. X.; Kohen, D. Molecular Insight into CO2 Trapdoor″ Adsorption in Zeolite Na-RHO. *Chem. Mater.* **2017**, *29* (7), 2724−2730.
(14) Ghojavand, S.; Dib, E.; Mintova, S. Flexibility in zeolites: origin, limits, and evaluation. *Chem. Sci.* **2023**, *14* (44), 12430−12446.
(15) Clatworthy, E. B.; Moldovan, S.; Nakouri, K.; Gramatikov, S. P.; Dalena, F.; Daturi, M.; Petkov, P. S.; Vayssilov, G. N.; Mintova, S. Visualizing the Flexibility of RHO Nanozeolite: Experiment and Modeling. *J. Am. Chem. Soc.* **2023**, *145* (28), 15313−15323.
(16) Clatworthy, E. B.; Paecklar, A. A.; Dib, E.; Debost, M.; Barrier, N.; Boullay, P.; Gilson, J.-P.; Nesterenko, N.; Mintova, S. Engineering RHO Nanozeolite: Controlling the Particle Morphology, Al and Cation Content, Stability, and Flexibility. *ACS Appl. Energy Mater.* **2022**, *5* (5), 6032−6042.
(17) Li, G.; Xiao, P.; Webley, P.; Zhang, J.; Singh, R.; Marshall, M. Capture of CO2 from high humidity flue gas by vacuum swing adsorption with zeolite 13X. *Adsorption* **2008**, *14* (2−3), 415−422.
(18) Kolle, J. M.; Fayaz, M.; Sayari, A. Understanding the effect of water on CO2 adsorption. *Chem. Rev.* **2021**, *121* (13), 7280−7345.
(19) Wang, Y.; LeVan, M. D. Adsorption equilibrium of binary mixtures of carbon dioxide and water vapor on zeolites 5A and 13X. *J. Chem. Eng. Data* **2010**, *55* (9), 3189−3195.
(20) Sircar, S.; Myers, A. L. Gas separation by zeolites. In *Handbook of Zeolite Science and Technology*; CRC Press, 2003; pp 1354−1406.
(21) Miyamoto, M.; Ono, S.; Kusukami, K.; Oumi, Y.; Uemiya, S. High Water Tolerance of a Core-Shell-Structured Zeolite for CO2 Adsorptive Separation under Wet Conditions. *ChemSusChem* **2018**, *11* (11), 1756−1760.
(22) Gao, F.; Li, Y.; Bian, Z.; Hu, J.; Liu, H. Dynamic hydrophobic hindrance effect of zeolite@ zeolitic imidazolate framework composites for CO 2 capture in the presence of water. *J. Mater. Chem. A* **2015**, *3* (15), 8091−8097.
(23) Thompson, J. A.; Zones, S. I. Binary- and Pure-Component Adsorption of CO2, H2O, and C6H14 on SSZ-13. *Ind. Eng. Chem. Res.* **2020**, *59* (40), 18151−18159.
(24) Zhou, Y.; Zhang, J.; Wang, L.; Cui, X.; Liu, X.; Wong, S. S.; An, H.; Yan, N.; Xie, J.; Yu, C.; et al. Self-assembled iron-containing mordenite monolith for carbon dioxide sieving. *Science* **2021**, *373* (6552), 315−320.
(25) Eubank, P. Estimation of effective molecular quadrupole moments. *AIChE J.* **1972**, *18* (2), 454−456.
(26) Pham, T. D.; Hudson, M. R.; Brown, C. M.; Lobo, R. F. Molecular basis for the high CO2 adsorption capacity of chabazite zeolites. *ChemSusChem* **2014**, *7* (11), 3031−3038.
(27) Pham, T. D.; Hudson, M. R.; Brown, C. M.; Lobo, R. F. On the Structure−Property Relationships of Cation-Exchanged ZK-5 Zeolites for CO2 Adsorption. *ChemSusChem* **2017**, *10* (5), 946−957.
(28) Lee, H.; Hikima, S.; Ohnishi, R.; Takewaki, T.; Katz, A. Privileged zeolitic sites for humid CO2 adsorption: K+ in double eight-membered rings. *Chem. Commun.* **2024**, *60* (74), 10140−10143.
(29) Xu, L.; Okrut, A.; Tate, G. L.; Ohnishi, R.; Wu, K. L.; Xie, D.; Kulkarni, A.; Takewaki, T.; Monnier, J. R.; Katz, A. Cs-RHO Goes from Worst to Best as Water Enhances Equilibrium CO2 Adsorption via Phase Change. *Langmuir* **2021**, *37* (47), 13903−13908.
(30) Lee, H.; Xie, D.; Zones, S. I.; Katz, A. CO2 Desorbs Water from K-MER Zeolite under Equilibrium Control. *J. Am. Chem. Soc.* **2024**, *146* (1), 68−72.
(31) Guo, X.; Corbin, D. R.; Navrotsky, A. Thermodynamics of H2O and CO2 Absorption and Guest-Induced Phase Transitions in Zeolite RHO. *J. Phys. Chem. C* **2018**, *122* (35), 20366−20376.

(32) Lozinska, M. M.; Mowat, J. P. S.; Wright, P. A.; Thompson, S. P.; Jorda, J. L.; Palomino, M.; Valencia, S.; Rey, F. Cation Gating and Relocation during the Highly Selective "Trapdoor" Adsorption of CO2 on Univalent Cation Forms of Zeolite Rho. *Chem. Mater.* **2014**, *26* (6), 2052−2061.
(33) Georgieva, V. M.; Bruce, E. L.; Verbraeken, M. C.; Scott, A. R.; Casteel, W. J.; Brandani, S.; Wright, P. A. Triggered Gate Opening and Breathing Effects during Selective CO2 Adsorption by Merlinoite Zeolite. *J. Am. Chem. Soc.* **2019**, *141* (32), 12744−12759.
(34) Choi, H. J.; Jo, D.; Min, J. G.; Hong, S. B. The Origin of Selective Adsorption of CO2 on Merlinoite Zeolites. *Angew. Chem., Int. Ed.* **2021**, *60* (8), 4307−4314.
(35) Korhonen, S. T.; Fickel, D. W.; Lobo, R. F.; Weckhuysen, B. M.; Beale, A. M. Isolated Cu2+ ions: active sites for selective catalytic reduction of NO. *Chem. Commun.* **2011**, *47* (2), 800−802.
(36) Luo, J.; Wang, D.; Kumar, A.; Li, J.; Kamasamudram, K.; Currier, N.; Yezerets, A. Identification of two types of Cu sites in Cu/SSZ-13 and their unique responses to hydrothermal aging and sulfur poisoning. *Catal. Today* **2016**, *267*, 3−9.
(37) Fu, D.; Park, Y.; Davis, M. E. Zinc Containing Small-Pore Zeolites for Capture of Low Concentration Carbon Dioxide. *Angew. Chem., Int. Ed. Engl.* **2022**, *61* (5), No. e202112916.
(38) Chester, A. W.; Derouane, E. G. *Zeolite Characterization and Catalysis*; Springer, 2009; Vol. *360*.
(39) Fang, H. J.; Kamakoti, P.; Zang, J.; Cundy, S.; Paur, C.; Ravikovitch, P. I.; Sholl, D. S. Prediction of CO2 Adsorption Properties in Zeolites Using Force Fields Derived from Periodic Dispersion-Corrected DFT Calculations. *J. Phys. Chem. C* **2012**, *116* (19), 10692−10701.
(40) Fang, H. J.; Kamakoti, P.; Ravikovitch, P. I.; Aronson, M.; Paur, C.; Sholl, D. S. First principles derived, transferable force fields for CO2 adsorption in Na-exchanged cationic zeolites. *Phys. Chem. Chem. Phys.* **2013**, *15* (31), 12882−12894.
(41) Andersen, C. W.; Bremholm, M.; Vennestrom, P. N. R.; Blichfeld, A. B.; Lundegaard, L. F.; Iversen, B. B. Location of Cu2+ in CHA zeolite investigated by X-ray diffraction using the Rietveld/maximum entropy method. *Iucrj* **2014**, *1*, 382−386.
(42) Sun, M. Y.; Nelson, A. E.; Adjaye, J. Examination of spinel and nonspinel structural models for γ-Al2O3 by DFT and Rietveld refinement simulations. *J. Phys. Chem. B* **2006**, *110* (5), 2310−2317.
(43) Smalley, C. J. H.; Hoskyns, H. E.; Hughes, C. E.; Johnstone, D. N.; Willhammar, T.; Young, M. T.; Pickard, C. J.; Logsdail, A. J.; Midgley, P. A.; Harris, K. D. M. A structure determination protocol based on combined analysis of 3D-ED data, powder XRD data, solid-state NMR data and DFT-D calculations reveals the structure of a new polymorph of l-tyrosine. *Chem. Sci.* **2022**, *13* (18), 5277−5288.
(44) Kresse, G.; Hafner, J. Ab-Initio Molecular-Dynamics Simulation of the Liquid-Metal Amorphous-Semiconductor Transition in Germanium. *Phys. Rev. B: Condens. Matter Mater. Phys.* **1994**, *49* (20), 14251−14269.
(45) Kresse, G.; Furthmuller, J. Efficient iterative schemes for ab initio total-energy calculations using a plane-wave basis set. *Phys. Rev. B: Condens. Matter Mater. Phys.* **1996**, *54* (16), 11169−11186.
(46) Hammer, B.; Hansen, L. B.; Norskov, J. K. Improved adsorption energetics within density-functional theory using revised Perdew-Burke-Ernzerhof functionals. *Phys. Rev. B: Condens. Matter Mater. Phys.* **1999**, *59* (11), 7413−7421.
(47) Coudert, F. X.; Vuilleumier, R.; Boutin, A. Dipole moment, hydrogen bonding and IR spectrum of confined water. *ChemPhysChem* **2006**, *7* (12), 2464−2467.
(48) Coudert, F. X.; Cailliez, F.; Vuilleumier, R.; Fuchs, A. H.; Boutin, A. Water nanodroplets confined in zeolite pores. *Faraday Discuss.* **2009**, *141*, 377−398.
(49) Boulfelfel, S. E.; Findley, J. M.; Fang, H. J.; Daou, A. S. S.; Ravikovitch, P. I.; Sholl, D. S. A Transferable Force Field for Predicting Adsorption and Diffusion of Small Molecules in Alkali Metal Exchanged Zeolites with Coupled Cluster Accuracy. *J. Phys. Chem. C* **2021**, *125* (48), 26832−26846.
(50) Findley, J. M.; Boulfelfel, S. E.; Fang, H. J.; Muraro, G.; Ravikovitch, P. I.; Sholl, D. S. A Transferable Force Field for Predicting Adsorption and Diffusion of Hydrocarbons and Small Molecules in Silica Zeolites with Coupled-Cluster Accuracy. *J. Phys. Chem. C* **2021**, *125* (15), 8418−8429.
(51) Chen, Z.; Berrens, M. L.; Chan, K.-T.; Fan, Z.; Donadio, D. Thermodynamics of water and ice from a fast and scalable first-principles neuroevolution potential. *J. Chem. Eng. Data* **2024**, *69* (1), 128−140.
(52) Chakarova, K.; Mihaylov, M.; Hadjiivanov, K. Can two CO2 molecules be simultaneously bound to one Na+ site in NaY zeolite? A detailed FTIR investigation. *Microporous Mesoporous Mater.* **2022**, *345*, 112270.
(53) Pulido, A.; Nachtigall, P.; Zukal, A.; Domínguez, I.; Cejka, J. Adsorption of CO_2 on Sodium-Exchanged Ferrierites: The Bridged CO_2 Complexes Formed between Two Extraframework Cations. *J. Phys. Chem. C* **2009**, *113* (7), 2928−2935.
(54) Pirngruber, G. D.; Raybaud, P.; Belmabkhout, Y.; Cejka, J.; Zukal, A. The role of the extra-framework cations in the adsorption of CO2 on faujasite Y. *Phys. Chem. Chem. Phys.* **2010**, *12* (41), 13534−13546.
(55) Zukal, A.; Pulido, A.; Gil, B.; Nachtigall, P.; Bludsky, O.; Rubes, M.; Cejka, J. Experimental and theoretical determination of adsorption heats of CO2 over alkali metal exchanged ferrierites with different Si/Al ratio. *Phys. Chem. Chem. Phys.* **2010**, *12* (24), 6413−6422.
(56) Nachtigall, P.; Delgado, M. R.; Nachtigallova, D.; Arean, C. O. The nature of cationic adsorption sites in alkaline zeolites-single, dual and multiple cation sites. *Phys. Chem. Chem. Phys.* **2012**, *14* (5), 1552−1569.
(57) Li, G. N.; Pidko, E. A. The Nature and Catalytic Function of Cation Sites in Zeolites: a Computational Perspective. *ChemCatChem* **2019**, *11* (1), 134−156.
(58) Ehrhardt, H.; Seidel, H.; Schweer, H. Hochdrucksynthesen einiger Carbonate mit überkritischem CO2. *Z. Anorg. Allg. Chem.* **1980**, *462* (1), 185−198.
(59) Bulánek, R.; Frolich, K.; Frýdová, E.; Čičmanec, P. Microcalorimetric and FTIR Study of the Adsorption of Carbon Dioxide on Alkali-Metal Exchanged FER Zeolites. *Top. Catal.* **2010**, *53* (19−20), 1349−1360.
(60) Bonelli, B.; Onida, B.; Fubini, B.; Arean, C. O.; Garrone, E. Vibrational and thermodynamic study of the adsorption of carbon dioxide on the zeolite Na−ZSM-5. *Langmuir* **2000**, *16* (11), 4976−4983.
(61) Bonelli, B.; Civalleri, B.; Fubini, B.; Ugliengo, P.; Areán, C. O.; Garrone, E. Experimental and quantum chemical studies on the adsorption of carbon dioxide on alkali-metal-exchanged ZSM-5 zeolites. *J. Phys. Chem. B* **2000**, *104* (47), 10978−10988.
(62) Datta, S. J.; Khumnoon, C.; Lee, Z. H.; Moon, W. K.; Docao, S.; Nguyen, T. H.; Hwang, I. C.; Moon, D.; Oleynikov, P.; Terasaki, O.; et al. CO2 capture from humid flue gases and humid atmosphere using a microporous coppersilicate. *Science* **2015**, *350* (6258), 302−306.
(63) Oda, A.; Hiraki, S.; Harada, E.; Kobayashi, I.; Ohkubo, T.; Ikemoto, Y.; Moriwaki, T.; Kuroda, Y. Unprecedented CO2 adsorption behaviour by 5A-type zeolite discovered in lower pressure region and at 300 K. *J. Mater. Chem. A* **2021**, *9* (12), 7531−7545.
(64) Coenen, K.; Gallucci, F.; Mezari, B.; Hensen, E.; van Sint Annaland, M. An in-situ IR study on the adsorption of CO2 and H2O on hydrotalcites. *J. CO2 Util.* **2018**, *24*, 228−239.
(65) Kock, E. M.; Kogler, M.; Bielz, T.; Klotzer, B.; Penner, S. In Situ FT-IR Spectroscopic Study of CO2 and CO Adsorption on Y2O3, ZrO2, and Yttria-Stabilized ZrO2. *J. Phys. Chem. C* **2013**, *117* (34), 17666−17673.
(66) Guo, P.; Shin, J.; Greenaway, A. G.; Min, J. G.; Su, J.; Choi, H. J.; Liu, L.; Cox, P. A.; Hong, S. B.; Wright, P. A.; et al. A zeolite family with expanding structural complexity and embedded isoreticular structures. *Nature* **2015**, *524* (7563), 74−78.

https://doi.org/10.1021/acs.chemmater.4c02496
Chem. Mater. 2024, 36, 11947−11957